

Supporting Information for “Investigating the Fast Response of Precipitation Intensity and Boundary Layer Temperature to Atmospheric Heating Using a Cloud-Resolving Model”

Xin Rong Chua¹, Yi Ming^{1,2}, Nadir Jeevanjee³

¹Program in Atmospheric and Oceanic Sciences, Princeton University, Princeton, New Jersey, USA

²Geophysical Fluid Dynamics Laboratory, Princeton, New Jersey, USA

³Department of Geosciences, Princeton University, Princeton, New Jersey, USA

Contents of this file

1. Text S1-2
2. Figures S1-S4
3. Table S1

Text S1. On the changes in near-surface relative humidity.

We elaborate on how the framework presented in the main text can be used to rationalize the changes in near-surface relative humidity. By manipulating Equations 1, 2, 5 and 6 of the main text,

$$\begin{aligned}\delta T_a &= \frac{1}{0.005c_p}(\delta RA_b + \alpha\delta RA_f) \\ \delta q_a &= \frac{1 - \alpha}{0.005L}\delta RA_f.\end{aligned}$$

In other words, for $0 < \alpha < 1$ (which is the case in our simulations), free-tropospheric radiative heating both warms and moistens the boundary layer, while boundary layer radiative heating warms the boundary layer. The change in near-surface RH can then be viewed as a competition between the two effects.

More quantitatively, assuming that changes in boundary layer saturation mixing ratio (denoted by q_a^*) follow Clausius-Clapeyron scaling, and denoting the constant for moist gas as $R_v = 461.5 \text{ J K}^{-1} \text{ kg}^{-1}$, we have

$$\delta q_a^* = \left(e^{\frac{L\delta T_a}{R_v(T_a + \delta T_a)T_a}} - 1 \right) q_a^*$$

The aforementioned equations allow us to make predictions of q_a and q_a^* in the heating experiments, which can then be used to calculate near-surface relative humidity ($RH_a = q_a/q_a^*$). Figure S1 shows the changes in RH_a diagnosed from the model against the predicted changes. As predicted, purely heating the boundary layer in B850 acts to decrease the relative humidity. In our simulations, free-tropospheric heating increases the relative humidity. Within each configuration, the change in HEAT is between that of A850 and B850, with the moistening effect winning out. One might suspect that this is simply because the heating in A850 vastly outweighs (is about 4.5 times that of) B850

(Table 1). Indeed, if we set $\delta RA_f = \delta RA_b$ in our calculations, our equations predict a decrease in RH_a .

Text S2. Changes in column-integrated re-evaporation (E)

We examine the relative importance of changes in domain-mean precipitation (P) versus changes in the fraction of precipitation that is re-evaporated (β) for understanding changes in column-integrated re-evaporation (E) under heating in our experiments. In Section 3.3, we explained that $E = (\frac{1}{\epsilon} - 1)P$, where ϵ is the precipitation efficiency. Since changes in $\frac{1}{\epsilon} - 1$ are small (less than 11%) in our experiments, $\frac{\delta E}{E} \approx \frac{\delta P}{P}$ (circles in Figure S4a). In other words, P is of leading order importance in understanding changes of E in our heating simulations.

Separately, Lutsko and Cronin (2018) (henceforth LC) proposed that β scales with the saturation deficit $1 - RH$ and the terminal fall speed w_f . This scaling can be linearized as:

$$\frac{\delta\beta}{\beta} = \frac{\delta(1 - RH)}{1 - RH} - \frac{\delta w_f}{w_f}. \quad (1)$$

Figure S4b shows the changes in β against the changes predicted by Equation 1. Following LC, $\beta = \frac{E}{E+P}$, and both RH and w_f are weighted by the amount of precipitating condensates at each level. Equation 1 holds reasonably well in our experiments; the best-fit line with no intercept has $R = 0.85$.

Since β is only one factor that influences E , changes in β need not be the leading explanation for changes in E . The crosses in Figure S4a illustrate that the RHS of Equation 1 underestimates the changes in re-evaporation in our experiments by more than a factor of two. Comparing the two scalings (circles versus crosses) confirms that P plays a larger role than β in influencing E in our experiments.

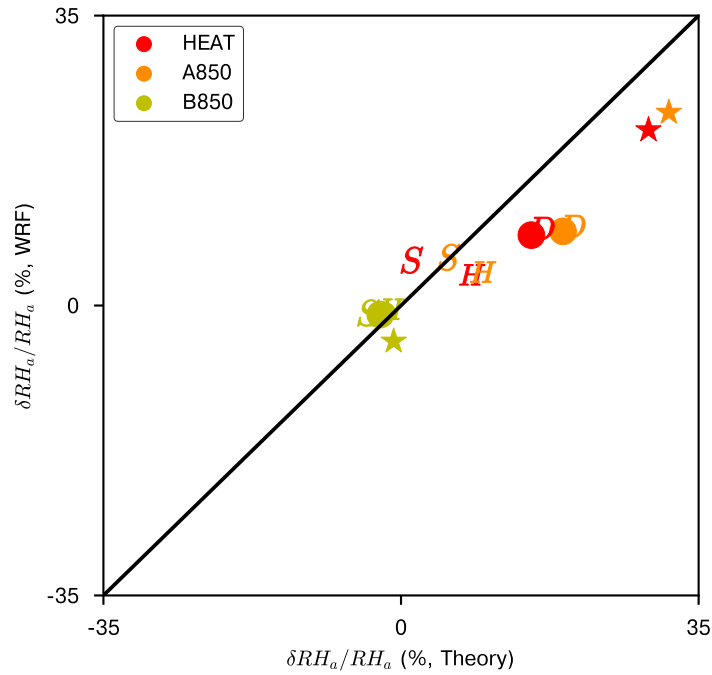


Figure S1. Percentage changes in relative humidity (RH_a) against percentage changes predicted by Text S1 (Theory). The best-fit slope with no-intercept is 0.64, with $R = 0.95$. Colors represent the different heating experiments (HEAT, A850, B850), and markers represent the default configuration (circles), those with partial re-evaporation (*), doubled domain size (D), half the radiative heating (H) and SSTs increased by 10 K (S).

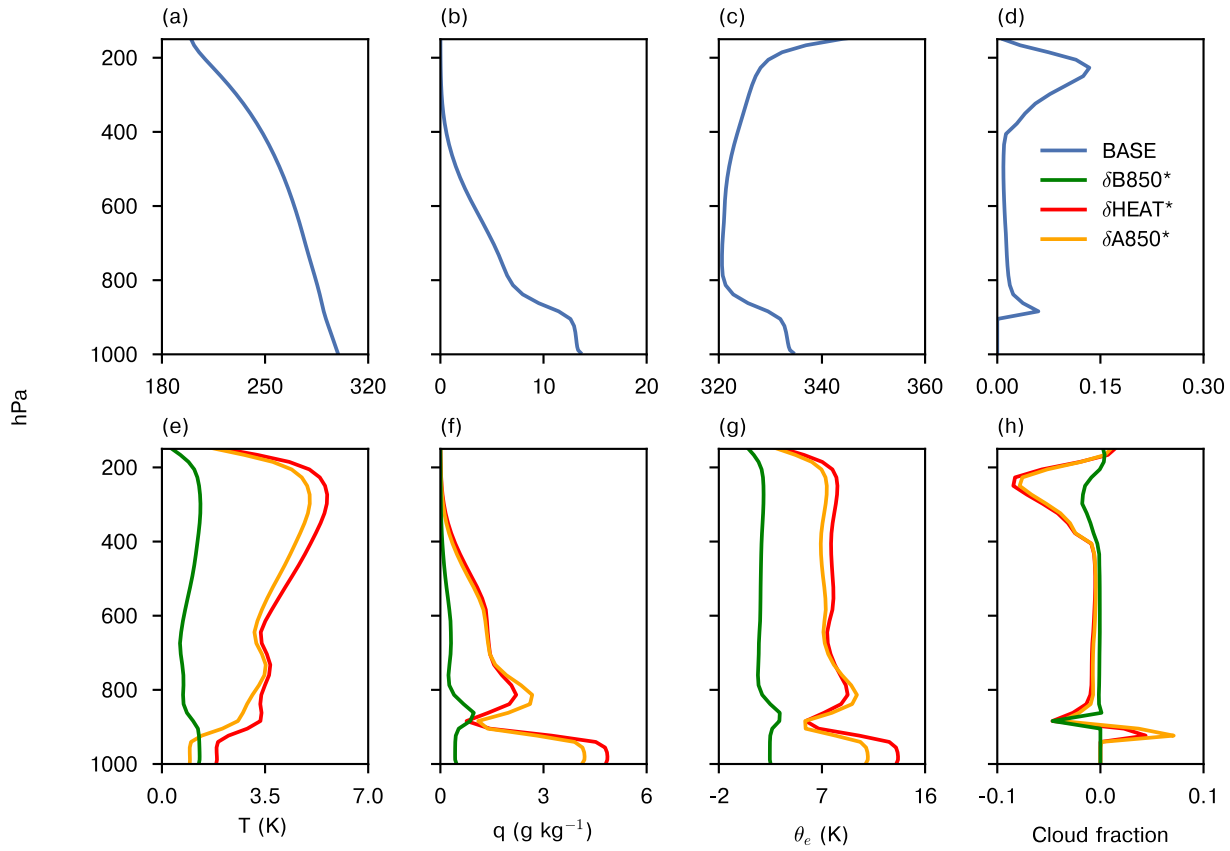


Figure S2. As in Figure 1, but for the partial re-evaporation experiments.

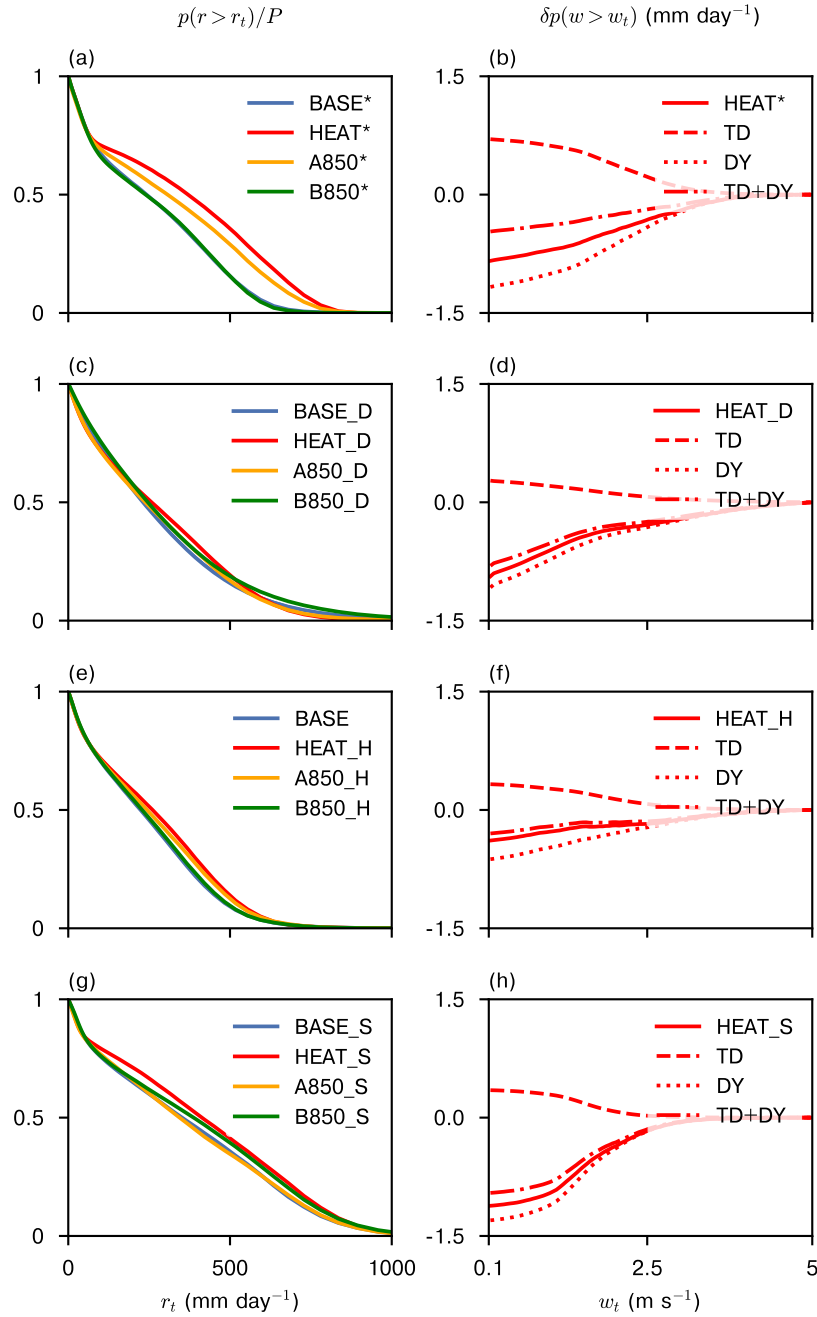


Figure S3. As in Figure 2b in the main text, but for experiments with (a) partial re-evaporation, (c) doubled domain size (D), (e) half the radiative heating (H), and SSTs increased by 10 K (S). (b,d,f,h) As in the first column, but for Figure 2f in the main text.

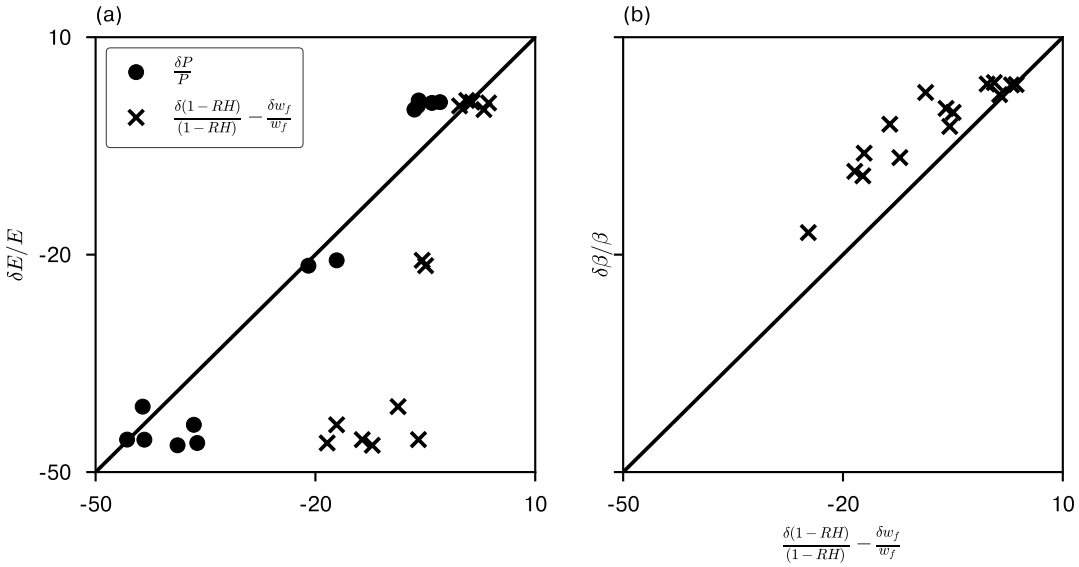


Figure S4. Scatter plots related to frameworks for changes in re-evaporation. The solid lines are the one-to-one lines. (a) Fractional changes in re-evaporation (E) against fractional changes in precipitation (P) (circles, best-fit slope with no-intercept of 1.1 and $R = 0.97$) and the sum of fractional changes in $1 - RH$ and the fall velocity (w_f), calculated as in Lutsko and Cronin (2018) (crosses, best-fit slope with no intercept of 2.8 and $R = 0.86$). (b) Fractional changes of the re-evaporation efficiency (β) against the sum of fractional changes in $1 - RH$ and the fall velocity (the same quantity as in (a)). The best-fit slope with no intercept is 0.47, with $R = 0.85$.

Table S1. Values of the 99.99th percentile of precipitation ($P_{99.99}$, mm day⁻¹) for each base configuration and the changes under HEAT ($\delta P_{99.99}$, %). BASE and BASE* are the full and partial re-evaporation experiments described in the text. In BASE_D (BASE_S), the domain size is doubled (sea surface temperatures are increased by 10 K).

Configuration	$P_{99.99}$	$\delta P_{99.99}$
BASE	654	-2.4
BASE*	653	15.9
BASE_D	843	-18.3
BASE_S	920	-4.2

References

Lutsko, N. J., & Cronin, T. W. (2018). Increase in precipitation efficiency with surface warming in radiative-convective equilibrium. *Journal of Advances in Modeling Earth Systems*.